Improving polymethacrylate EUV resists with TiO_2 area-selective deposition

Rachel A. Nye*[a,b,c], Kaat Van Dongen[b,c], Hironori Oka[d], Hajime Furutani[d], Gregory Parsons[a], Danilo De Simone[c], Annelies Delabie[b,c]

[a] North Carolina State University, 911 Partners Way, Raleigh, NC, USA 27606; [b] KU Leuven (University of Leuven), Leuven, Belgium; [c] IMEC, Kapeldreef 75, B-3001 Leuven, Belgium; [d] FUJIFILM Corporation Electronic Materials Research Laboratories, Kawashiri 4000, Yoshida-Cho, Haibara-Gun, Shizuoka, Japan

ABSTRACT

Extreme ultraviolet (EUV) lithography is crucial to achieving smaller device sizes for next-generation technology, although organic resists face substantial challenges, such as low etch resistance, which limit the resolution of smaller features. Area-selective deposition (ASD) is one potential avenue to improve pattern resolution from organic EUV resists by selectively depositing material on one region of the resist, while preventing material deposition on an adjacent region. We therefore evaluate the compatibility of various organic EUV resists with area-selective atomic layer deposition (ALD) processes, including considering the effects of photo-acid generator (PAG) and EUV exposure on polymer properties and selectivity. The thermal stability of thin resist materials at the TiO_2 deposition temperature (125ºC for 60 minutes) is confirmed with water contact angle and atomic force microscopy. Upon TiO_2 ALD from $TiCl_4$ and H_2O, Rutherford backscattering spectrometry reveals successful TiO_2 deposition on poly(*tert*-butyl methacrylate), poly(p-hydroxystyrene), and poly(p-hydroxystyrene-random-methacrylic acid) polymers, regardless of PAG or EUV exposure. However, TiO_2 inhibition is observed on poly(cyclohexyl methacrylate). Thus, we demonstrate that EUV polymers can serve as either the growth or non-growth surface during TiO_2 ASD, an insight that can be used to enable resist hardening and tone inversion applications, respectively. These results serve as a basis for further ASD studies on EUV resist materials to improve pattern resolution in next-generation devices.

Keywords: EUV lithography, Photoresist, Area-selective deposition, ALD, TiO_2, Polymethacrylate

1. INTRODUCTION

As semiconductor manufacturing approaches next-generation technology nodes (< 7 nm), the need for high-NA extreme ultraviolet (EUV) lithography is becoming increasingly apparent.[1] One of the biggest obstacles is the development of resist materials that can simultaneously improve pattern resolution, line-edge roughness (LER), and sensitivity, i.e. the RLS triangle.[2–4] Commonly used chemically amplified resists (CARs) could benefit from the addition of a material with higher etch resistance to improve resolution and LER. Another potential method to improve CAR performance is via tone inversion. This would be especially helpful to convert from positive tone resists, which are typically easier to fabricate, to negative tone patterns, which typically result in higher resolution, lower LER, and less pattern collapse during pattern transfer.[4–6] One advancing technique that has potential to improve patterning processes in the aforementioned ways and thus greatly improve EUV lithography performance is area-selective deposition (ASD).[7–9]

ASD is a bottom-up nanopatterning technique that exploits chemical differences on a surface to deposit material on one region without depositing on an adjacent region.[8,10] This is typically achieved with chemical vapor deposition (CVD) or atomic and molecular layer deposition (ALD/MLD), the latter of which relies on self-limiting vapor-solid surface reactions to deposit material with nanoscale thickness control.[8,10–12] Thus, an area-selective ALD/MLD process is highly controllable in terms of deposited layer thickness and conformality.[13] Combining ASD with EUV lithography could improve layer alignment, reduce edge placement error and reduce the height requirements in 3D stacks.[14–16] Thus, area-selective ALD shows promise for depositing etch-resistant layers on EUV resists to enable tone inversion or resist

hardening to improve pattern resolution, as shown schematically in Figure 1.[14,17,18] TiO_2 is one ASD-compatible material of particular interest for its high etch resistance, chemical stability, and compatibility with low-temperature (~100 ºC) processing.[19,20] This film has high reactivity with OH surface groups, such as those expected on exposed resist surfaces. Furthermore, TiO_2 ALD has demonstrated excellent selectivity in many ASD processes, including on substrates such as amorphous carbon, H-terminated Si, SiO_2, TiO_2, Ru, and TiN.[15,21] Despite these benefits, studies of TiO_2 on EUV resist materials so far focus mainly on layers thicker than 100 nm, while much thinner materials are needed for patterning with high NA EUV lithography.[9,22]

In this work, we investigate the compatibility between TiO_2 ALD and ~30 nm thin EUV resist materials for use in ASD of a resist-hardening or tone-inverting layer. We first evaluate the thermal compatibility of ~30 nm organic photoresist materials with the TiO_2 ALD temperature window. Moreover, we systematically consider the effects of resist additives (e.g. PAG and EUV exposure) on surface hydrophobicity and roughness at ALD temperatures. Next, we determine the TiO_2 growth rate and $TiCl_4$ precursor reactivity on several resist materials, again discussing the impact of PAG and EUV exposure on ALD. Finally, we investigate how the polymer protecting group influences the TiO_2 growth rate, and discuss potential applications for each resist material. We utilize this insight to identify relevant challenges and future directions to pave the way for effective collaborations between ASD and EUV lithography.

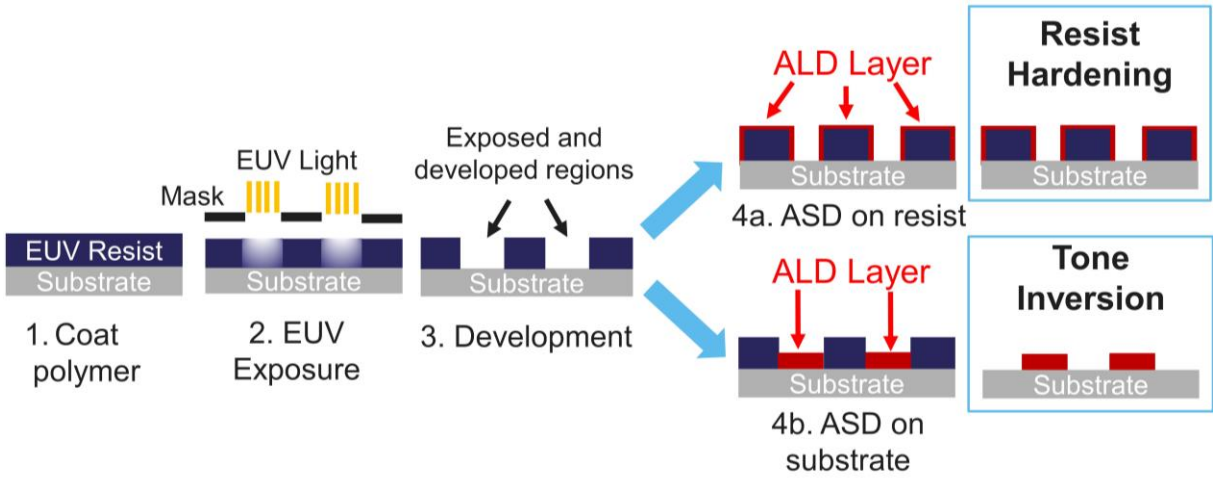

Figure 1. Schematic of EUV lithographic patterning (in this case on positive tone resist) in conjunction with ASD for resist hardening or tone inversion applications.

2. METHODOLOGY

The EUV resist materials used in this work are provided by Fujifilm and consist of organic polymers with methacrylate backbones and various protecting groups, as shown in Figure 2. We focus on poly(*tert*-butyl methacrylate) (PtBuMA), poly(p-hydroxystyrene) (PHS), poly(p-hydroxystyrene-random-methacrylic acid) (P(HS-r-MAA)), and poly(cyclohexyl methacrylate) (PCHMA). In some experiments, a photo-acid generator (PAG), 4-(methylphenyl) diphenylsulfonium nonaflate, is also incorporated into the polymers, with the PAG structure shown in Figure 2. Polymers are spin-coated to ~30 nm on SiO_2 substrates primed with hexamethyldisilazane (HMDS). A post-apply bake (PAB) is utilized at 120 ºC for 90 s. In some experiments, the polymers are then exposed to 15 mJ/cm^2 EUV light and undergo a post-exposure bake (PEB) at 120 ºC for 90 s. Exposed regions are ~2 cm x ~3 cm. Development is not utilized in this work. TiO_2 is deposited via ALD (Polygon 8300 EmerALD) with $TiCl_4$ and H_2O at 125 ºC on blanket exposed or unexposed regions of the resist materials.

Polymer materials are characterized using Fourier transform infrared spectroscopy (FTIR, Nicolet 6700 Spectrometer from Thermoelectron Corporation), water contact angle (WCA, Dataphysics OCAH 230) and atomic force microscopy

(AFM, Bruker Dimension Edge). The Ti content on the polymers is quantified using Rutherford backscattering spectrometry (RBS, 1.523 MeV He^+ ion beam).

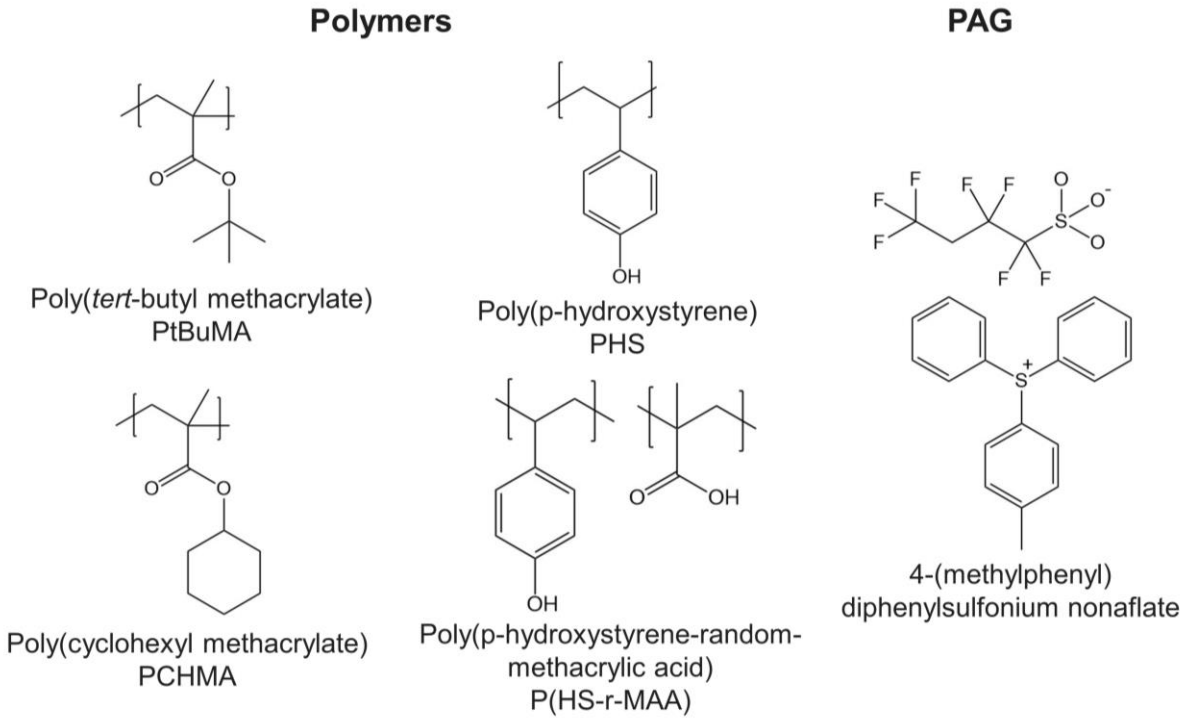

Figure 2. Structures for each polymer and PAG utilized in this work.

3. RESULTS AND DISCUSSION

3.1 EUV Polymer Resist Characterization – Compatibility with ALD

We first discuss chemical changes expected from the PtBuMA polymer upon addition of PAG and exposure to EUV light. Figure 3a shows the structure of the PtBuMA resist before and after exposure, where EUV light causes the methyl-terminated surface (hydrophobic) to convert to a hydroxyl-terminated surface (hydrophilic).[22] This transition is confirmed with FTIR results in Figure 3b. Specifically, we note the conversion of the CH_3 stretching peak (~3000 cm^{-1}) for the unexposed PtBuMA polymers (both with and without PAG) to an OH stretching peak (~2800-3300) after exposure and PEB. Additionally, the $C(CH_3)$ stretch at ~1370 cm^{-1} disappears after exposure, and the peak at ~1720 cm^{-1} before exposure (COOR) is shifted to ~1700 cm^{-1} after exposure (COOH). This difference in surface properties is expected to cause a difference in the rate of TiO_2 nucleation during ASD, thus enabling faster growth on the exposed, hydrophilic surface while inhibiting growth on the unexposed, hydrophobic surface.

Next, we evaluate the PtBuMA, PHS, and P(HS-r-MAA) polymer surface properties at typical ALD temperatures (100-200^{o}C) to determine polymer thermal compatibility. The spin-coated polymers are examined using three conditions: 1) without PAG, 2) with PAG, and 3) with PAG after exposure and PEB. To simulate an ALD process, the polymers are placed in an oven for 60 minutes at various temperatures between 90-180^{o}C under lab air ambient environment. The annealed surfaces are analyzed using WCA to measure surface hydrophobicity and AFM to measure surface roughness, with results shown in Figure 4 and 5, respectively.

Figure 4 shows the WCA of each polymer under different conditions. As spin-coated, the methyl-terminated PtBuMA has the highest WCA (~88^o), while the hydroxyl-terminated PHS and P(HS-r-MAA) polymers have a lower contact angle around 59^o, as seen in Figure 4a. All HS-based polymers are thermally stable up to 180^{o}C, as there is no significant

change in WCA upon annealing. We note a small decrease in WCA for PtBuMA when it is heated above 135ºC. When PAG is incorporated (Fig. 4b), the polymers undergo a similar trend, where the PtBuMA has the highest WCA (~82º) as spin-coated compared to PHS and P(HS-r-MAA) (~63º) and no significant change in WCA is observed after annealing up to 135ºC. After exposing the samples with PAG to EUV light (Fig. 4c), the PHS and P(HS-r-MAA) polymers maintain the same WCA (~60º) and are not affected by annealing up to 135ºC. However, the exposed PtBuMA shows different behavior. The WCA decreases to ~33º after exposure and before annealing, consistent with the conversion of surface tBu groups to OH groups during exposure. For this material, the WCA does not significantly change during annealing until 150ºC, where the WCA increases to ~60º. This indicates poor thermal stability for the exposed PtBuMA polymer starting around 150ºC. The difference in stability for exposed versus unexposed resist highlights an important challenge in conducting ASD on EUV resists, as associated lithographic processing (e.g. addition of PAG, exposure, etc.) may affect the resist surface properties relevant to ASD.

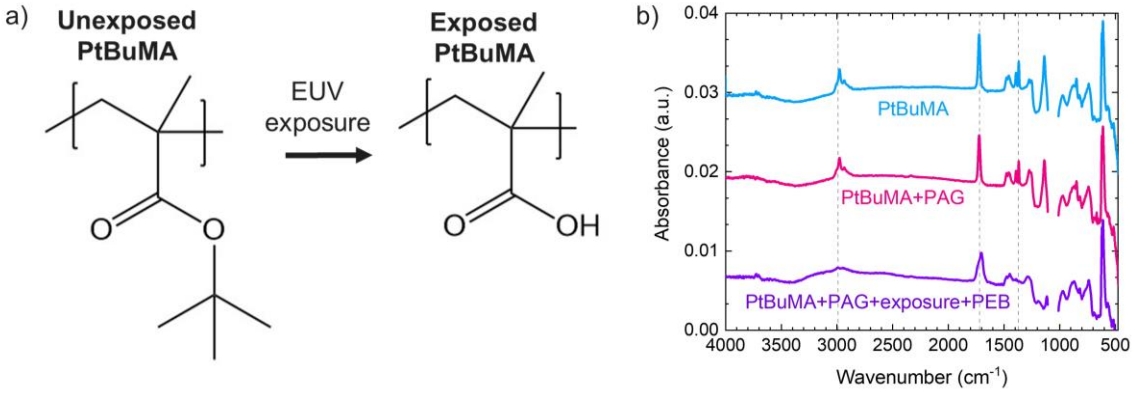

Figure 3. (a) Structure of the PtBuMA polymer before and after EUV exposure, showing conversion from tBu to OH groups. (b) FTIR spectra of PtBuMA only (blue), PtBuMA with PAG (pink), and PtBuMA with PAG after exposure and PEB (purple). Relevant peaks are indicated. Si-O peak at ~1100 cm^{-1} is omitted for clarity.

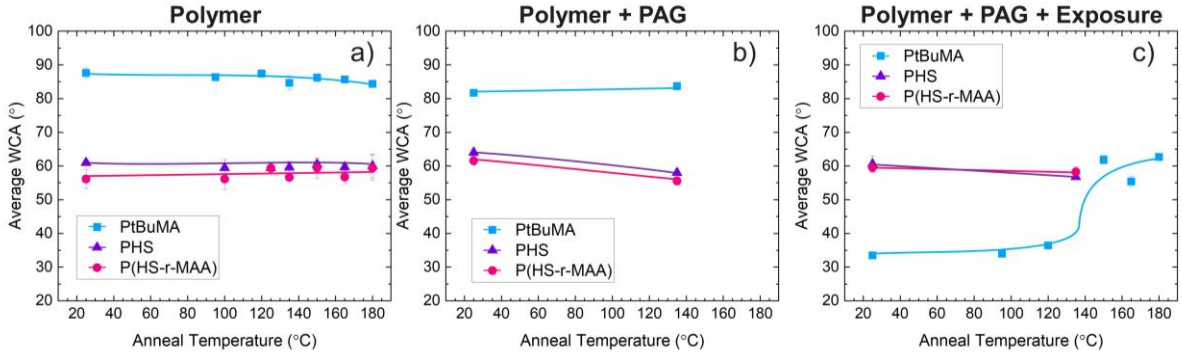

Figure 4. Water contact angle measurements for PtBuMA (blue squares), PHS (purple triangles), and P(HS-r-MAA) (pink circles) as a function of anneal temperature for samples of (a) polymers without PAG, (b) polymers with PAG, and (c) polymers with PAG after exposure and PEB. Lines are drawn as guides to the eye.

Figure 5 shows RMS surface roughness measured by AFM, which is used to further characterize the thermal stability of the polymers. For as spin-coated polymers without PAG (Fig. 5a), we observe that the PtBuMA has a much higher surface roughness (~0.6 nm) compared to PHS or P(HS-r-MAA) (<0.3 nm). The roughness of the hydroxyl-terminated polymers does not change during annealing, consistent with WCA results (Figure 4). On the other hand, the roughness of PtBuMA decreases significantly to ~0.3 nm after annealing at 95ºC, but increases again to ~1.1 nm at 150ºC (consistent with the slight decrease in WCA observed in Figure 4a at 150ºC). Upon addition of PAG to the PtBuMA sample (Fig. 5b), the RMS roughness undergoes the same trend, decreasing from ~0.6 to ~0.3 nm after annealing at 135ºC. However,

after exposing the PtBuMA+PAG sample (Fig. 5b), the surface roughness increases dramatically to ~1.3 nm before annealing and decreases to ~0.7 nm after annealing between 95 – 180 ºC. Thus, despite a stable contact angle for the PtBuMA surfaces up to ~135ºC, the RMS roughness varies significantly upon annealing as low as 95ºC.

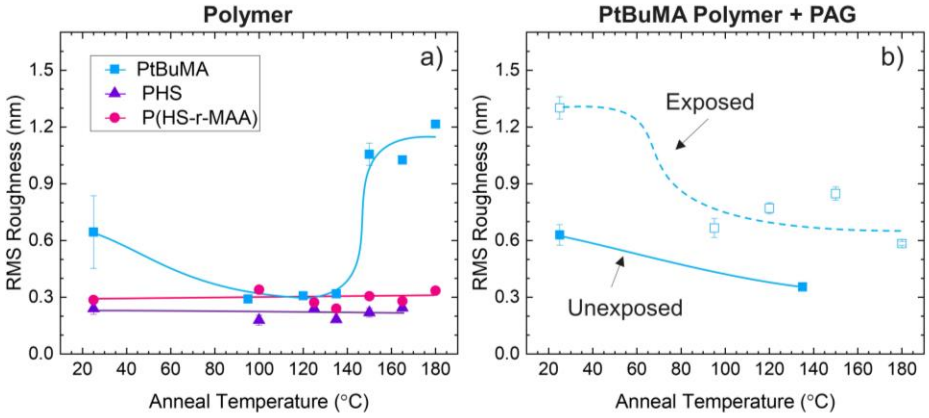

Figure 5. RMS roughness measurements from AFM for PtBuMA (blue squares), PHS (purple triangles), and P(HS-r-MAA) (pink circles) as a function of anneal temperature for samples of (a) polymers without PAG and (b) PtBuMA with PAG before (filled shapes) and after (open shapes) exposure and PEB. Lines are drawn as guides to the eye.

Figure 6 shows morphological changes on PtBuMA from AFM topographical scans over a 1 μm x 1 μm area. Without PAG, the surface is relatively smooth and homogeneous (Fig. 6a). When incorporating the PAG into the polymer (Fig. 6b), some darker regions appear on the image, corresponding to holes in the surface which are attributed to some phase separation between the hydrophobic polymer and the PAG. After exposure (Fig. 6c), these darker regions have increased in frequency and intensity, indicating large craters across the polymer surface. These craters measure approximately 80-160 nm wide and 3-9 nm deep, which is close to the average exposed film thickness of 10-15 nm (according to ellipsometry). XPS (not shown) reveals an increase in Si concentration detected on these exposed samples, suggesting that the craters formed on the exposed PtBuMA+PAG surface reach close to the underlying Si substrate. Inconsistent surfaces are problematic for ASD, thus future work should seek to reduce the problem of phase separation in resist materials, for example by utilizing copolymer samples of the tBuMA component with PAG. Based on these findings, we choose to deposit TiO_2 at 125ºC to represent a reasonable processing temperature for ALD where minimal changes are apparent in WCA and surface roughness for as-deposited and annealed polymers.

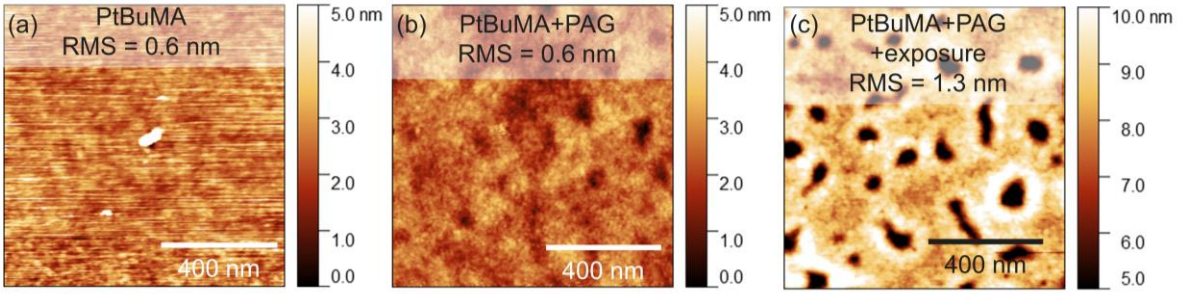

Figure 6. Topographical images from AFM over 1 μm x 1 μm areas for PtBuMA (a) without PAG, (b) with PAG, and (c) with PAG after exposure and PEB. Note the z-scale increases from 5 nm in (a) and (b) to 10 nm in (c).

3.2 TiO_2 ALD on Exposed vs Unexposed Polymers

Using a previously established TiO_2 ALD process,[21] we deposit various cycle numbers of TiO_2 on each polymer (with and without PAG and before and after exposure) to evaluate the potential for selective deposition. Surfaces are then analyzed with WCA and Rutherford backscattering spectrometry (RBS) to measure surface hydrophobicity and Ti

content, respectively. Figure 7 shows WCA measurements taken after various TiO_2 cycle numbers to compare changes in surface hydrophobicity. For all unexposed polymers (both with and without PAG), the WCA decreases with increasing ALD cycle, corresponding to a decrease in hydrophobicity consistent with TiO_2 (WCA~60º) depositing on the surface. After 100 cycles of ALD on PtBuMA, the contact angle has dropped to < ~30º, consistent with the formation of a TiO_2 film. For polymers with OH terminations (PHS and P(HS-r-MAA)), this decrease in WCA is already notable over the first 50 cycles, corresponding to the largest change in surface composition from polymer to TiO_2. The presence of PAG for these polymers results in a somewhat slower decrease in contact angle. When conducting ALD on these exposed polymers with PAG, the WCA decreases even more slowly. In contrast, PAG addition results in a more rapid decrease in WCA for PtBuMA. For the exposed PtBuMA, the WCA after exposure is already quite small (~35º), and therefore does not change significantly during TiO_2 deposition.

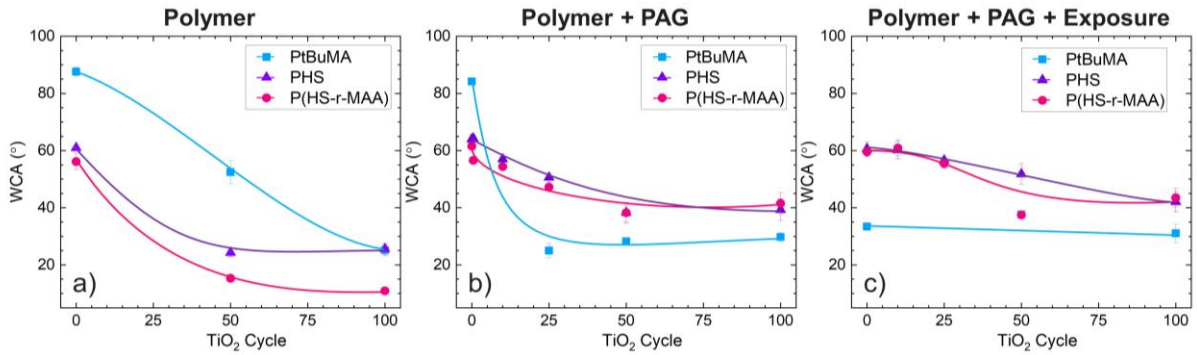

Figure 7. WCA measurements after various cycles of TiO_2 ALD from $TiCl_4$ and H_2O at 125ºC on PtBuMA (blue squares), PHS (purple triangles), and P(HS-r-MAA) (pink circles) for samples of (a) polymers without PAG, (b) polymers with PAG, and (c) polymers with PAG after exposure and PEB. Lines are drawn as guides to the eye.

Figure 8 shows the amount of deposited TiO_2 as measured by RBS. From the Ti aerial density, the equivalent TiO_2 thickness is calculated using 3.72 g/cm^3 TiO_2 density. For polymers without PAG, Ti content increases with increasing cycle number at a rate comparable to the expected TiO_2 growth rate on an SiO_2 surface (i.e. 0.037 nm/cycle), consistent with previous results.[8,9] This leads to ~4 nm TiO_2 deposited on each surface after 100 ALD cycles. Upon addition of PAG, the TiO_2 growth per cycle (GPC) decreases somewhat for each film to ~0.025 nm/cycle. The same ~0.025 nm/cycle growth rate is observed on each polymer after exposure, despite the difference in initial WCA on each surface (Fig. 4 and 7). These trends in Ti uptake are consistent with trends in WCA from Figure 7. The exact mechanisms causing TiO_2 growth on each polymer (in particular despite hydrophobic surfaces) should be investigated in future work.

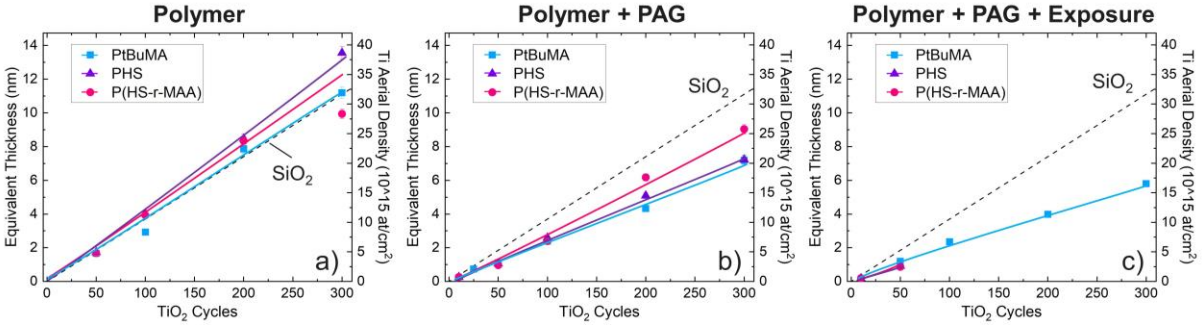

Figure 8. RBS measurements of equivalent TiO_2 film thickness (left y-axis) calculated from Ti content (right y-axis) for various cycles of TiO_2 deposited from $TiCl_4$ and H_2O at 125ºC on PtBuMA (blue squares), PHS (purple triangles), and P(HS-r-MAA) (pink circles) for samples of (a) polymers without PAG, (b) polymers with PAG, and (c) polymers with PAG after exposure and PEB. Lines are drawn as guides to the eye. TiO_2 ALD on SiO_2 is included as black dashed line for reference.

Thus, TiO_2 is successfully deposited on PtBuMA, PHS, and P(HS-r-MAA) polymers regardless of the presence of PAG or EUV exposure. This indicates that an etch-resistant TiO_2 layer could be successfully deposited on the remaining resist after development (in either a positive or negative tone process). If the underlying substrate inhibits TiO_2 growth (e.g. passivated SiO_2 or SiH), then this selective deposition will result in a hardened resist.

To evaluate how the $TiCl_4$ precursor initially reacts with the polymer surfaces during ALD, we verify the self-limiting nature of the surface reaction by repeating $TiCl_4$ doses 1 and 10 times on the surface of P(HS-r-MAA) and perform RBS measurements to determine resulting Ti content. In an ideal ALD process, once all available surface sites have reacted, no more material will be added to the surface. RBS results in Figure 9 show that increased $TiCl_4$ doses result in approximately the same Ti content regardless of PAG or exposure. This indicates that $TiCl_4$ reacts with all available surface OH sites and there is no significant $TiCl_4$ physisorption or sub-surface diffusion on this polymer. We note that this self-limiting behavior of $TiCl_4$ may vary for deposition on different polymers, for example on PtBuMA that does not have reactive OH sites on the surface.[9,23] These insights will be important to identifying causes of selectivity loss on polymers and developing strategies to inhibit TiO_2 growth on undesired regions.

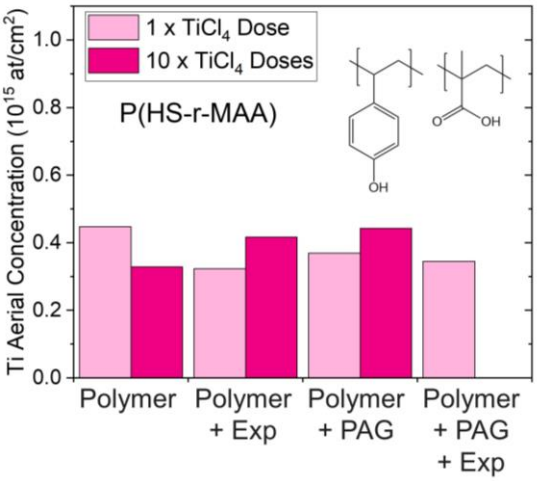

Figure 9. RBS measurements of the Ti content after one and ten $TiCl_4$ doses on P(HS-r-MAA) with and without PAG and before and after exposure and PEB.

3.3 TiO_2 ALD on Polymers with Varied Protecting Groups

We next consider TiO_2 ALD on a methacrylate-based polymer with a different protecting group, specifically poly(cyclohexyl methacrylate) (PCHMA). Figure 10 shows RBS results during TiO_2 ALD at 125ºC, with PtBuMA shown for reference. Interestingly, we observe a substantial delay in the TiO_2 deposition on this modified polymer material. Compared to the 0.029 nm/cycle GPC on PtBuMA, the initial growth rate on PCHMA is much lower, yielding only ~0.5 nm TiO_2 after 100 cycles (compared to ~2.9 nm on PtBuMA or ~3.7 nm on SiO_2). This initial growth inhibition on PCHMA could be due to the bulkier protecting group or the different bonding structure compared to the polymers containing tBuMA and MAA. Using the definition of selectivity (S) in Equation 1, where t represents the thickness on the growth (G, i.e. PCHMA) and non-growth (NG, i.e. SiO_2 substrate) surfaces, respectively,[7] this result corresponds to a selectivity of ~76% after 100 cycles.

$$S \cong (t_G - t_{NG}) / (t_G + t_{NG}) \qquad \text{Equation 1}$$

Thus, these results show that varying the resist structure is a viable way to induce selectivity during TiO_2 ALD. In this example, the structure of the PCHMA polymer shows promise for inhibiting deposition on a resist surface. For a positive-tone resist, this could be used for tone inversion either before development (deposition on exposed resist selective to unexposed resist) or after development (deposition on substrate selective to unexposed resist). Overall, the results presented here confirm the potential for ASD to be used successfully on thin polymers for EUV resist materials.

Additional work is needed to expand these results to copolymers and identify relevant selectivity loss mechanisms on resist materials.

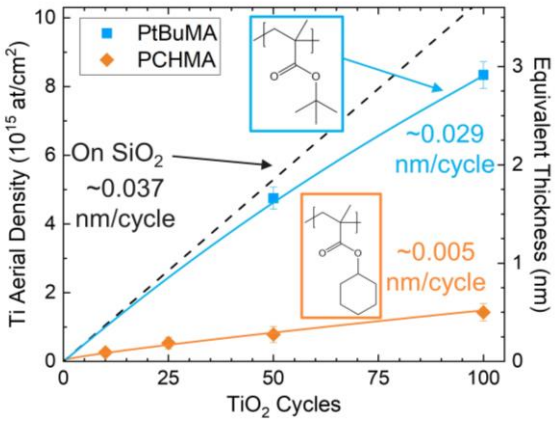

Figure 10. RBS measurements of Ti content (left y-axis) and equivalent TiO_2 film thickness (right y-axis) for various cycles of TiO_2 deposited from $TiCl_4$ and H_2O at 125ºC on PtBuMA (blue squares) and PCHMA (orange diamonds). Lines are drawn as guides to the eye. TiO_2 ALD on SiO_2 is included as black dashed line for reference.

4. CONCLUSIONS

In this work, we successfully demonstrate the compatibility of TiO_2 area-selective deposition with ~30 nm thin EUV resist materials. WCA and AFM measurements demonstrate thermal stability of PtBuMA, PHS, and P(HS-r-MAA) polymers at the required operating temperatures for TiO_2 ALD (i.e. 125ºC). We emphasize the importance of characterizing resist materials with all required resist components (e.g., with PAG and EUV exposure), as these factors have important impacts on resist surface properties and thermal stability for ASD. TiO_2 is successfully deposited on each of these polymers regardless of PAG or exposure, making them promising candidates for resist hardening applications performed after development on a substrate that inhibits TiO_2 deposition. On the other hand, TiO_2 deposition on PCHMA is inhibited for the first 100 ALD cycles, making this an interesting option for tone inversion applications. We achieve 76% selectivity after 100 ALD cycles on PCHMA relative to the SiO_2 substrate, resulting in a TiO_2 film of ~3.7 nm on SiO_2. Thus, we conclude that TiO_2 ASD is compatible with organic EUV resist processing, and we furthermore demonstrate successful selectivity of TiO_2 between different types of polymers. Future work is needed to expand TiO_2 ASD to additional polymers, copolymers, and to elucidate the resist characteristics that enable or inhibit TiO_2 ALD.

ACKNOWLEDGEMENTS

The authors would like to thank Nadia Vandenbroeck for her insightful discussions and material processing.

REFERENCES

(1) Li, L.; Liu, X.; Pal, S.; Wang, S.; Ober, C. K.; Giannelis, E. P. Extreme Ultraviolet Resist Materials for Sub-7 Nm Patterning. *Chem. Soc. Rev.* **2017**, *46*, 4855–4866.

(2) Higgins, C. D.; Szmanda, C. R.; Antohe, A.; Denbeaux, G.; Georger, J.; Brainard, R. L. Resolution, Line-Edge Roughness, Sensitivity Tradeoff, and Quantum Yield of High Photo Acid Generator Resists for Extreme Ultraviolet Lithography. *Jpn. J. Appl. Phys.* **2011**, *50* (036504).

(3) Mojarad, N.; Gobrecht, J.; Ekinci, Y. Beyond EUV Lithography: A Comparative Study of Efficient Photoresists' Performance. *Sci. Rep.* **2015**, *5* (9235).

(4) Fujimori, T.; Tsuchihashi, T.; Itani, T. Recent Progress of Negative-Tone Imaging Process and Materials with EUV Exposure. In *Proc. of SPIE*; 2015; Vol. 9425, p 942505.
(5) Sixt, C. Surface Functionalisation of Extreme Ultraviolet Photoresist Material for Area-Selective Deposition, 2019.
(6) Tsubaki, H.; Nihashi, W.; Tsuchihashi, T.; Yamamoto, K.; Goto, T. Negative-Tone Imaging with EUV Exposure toward 13nm Hp. In *Proc. of SPIE*; SPIE, 2016; Vol. 9776, p 977608.
(7) Parsons, G. N.; Clark, R. D. Area-Selective Deposition: Fundamentals, Applications, and Future Outlook. *Chem. Mater.* **2020**, *32* (12), 4920–4953.
(8) Song, S. K.; Saare, H.; Parsons, G. N. Integrated Isothermal Atomic Layer Deposition/Atomic Layer Etching Supercycles for Area-Selective Deposition of TiO2. *Chem. Mater.* **2019**, *31* (13), 4793–4804.
(9) Sinha, A.; Hess, D. W.; Henderson, C. L. Area Selective Atomic Layer Deposition of Titanium Dioxide: Effect of Precursor Chemistry. *J. Vac. Sci. Technol. B* **2006**, *24* (6), 2523.
(10) Grillo, F.; Soethoudt, J.; Marques, E. A.; De Martín, L.; Van Dongen, K.; Ruud Van Ommen, J.; Delabie, A. Area-Selective Deposition of Ruthenium by Area-Dependent Surface Diffusion. *Chem. Mater.* **2020**, *32* (22), 9560–9572.
(11) Nye, R. A.; Wang, S.; Uhlenbrock, S.; Smythe, J. A. I.; Parsons, G. N. In Situ Analysis of Growth Rate Evolution during Molecular Layer Deposition of Ultra-Thin Polyurea Films Using Aliphatic and Aromatic Precursors. *Dalt. Trans.* **2022**, *51* (5), 1838–1849.
(12) Nye, R. A.; Kelliher, A. P.; Gaskins, J. T.; Hopkins, P. E.; Parsons, G. N. Understanding Molecular Layer Deposition Growth Mechanisms in Polyurea via Picosecond Acoustics Analysis. *Chem. Mater.* **2020**, *32* (4), 1553–1563.
(13) Kim, J.-S.; Parsons, G. N. Nanopatterned Area-Selective Vapor Deposition of PEDOT on SiO 2 vs Si-H: Improved Selectivity Using Chemical Vapor Deposition vs Molecular Layer Deposition. *Chem. Mater.* **2021**, *33* (23), 9221–9230.
(14) Clark, R.; Tapily, K.; Yu, K.-H.; Hakamata, T.; Consiglio, S.; O'Meara, D.; Wajda, C.; Smith, J.; Leusink, G. Perspective: New Process Technologies Required for Future Devices and Scaling. *APL Mater.* **2018**, *6* (5), 058203.
(15) Soethoudt, J.; Tomczak, Y.; Meynaerts, B.; Chan, B. T.; Delabie, A. Insight into Selective Surface Reactions of Dimethylamino-Trimethylsilane for Area-Selective Deposition of Metal, Nitride, and Oxide. *J. Phys. Chem. C* **2020**, *124* (13), 7163–7173.
(16) Wojtecki, R.; Ma, J.; Cordova, I.; Arellano, N.; Lionti, K.; Magbitang, T.; Pattison, T. G.; Zhao, X.; Delenia, E.; Lanzillo, N.; et al. Additive Lithography–Organic Monolayer Patterning Coupled with an Area-Selective Deposition. *ACS Appl. Mater. Interfaces* **2021**, *13* (7), 9081–9090.
(17) Van Dongen, K.; De Simone, D.; Delabie, A. Surface Passivation Using Aminosilanes for Area-Selective Atomic Layer Deposition and Extreme Ultraviolet Lithography, 2020.
(18) Yao, H.; Mullen, S.; Wolfer, E.; Mckenzie, D.; Dioses, A.; Rahman, D.; Cho, J.; Padmanaban, M.; Petermann, C.; Hong, S.; et al. Spin-on Metal Oxides and Their Applications for Next Generation Lithography. *J. Photopolym. Sci. Technol.* **2016**, *29* (1), 59–67.
(19) Park, M. H.; Jang, Y. J.; Sung-Suh, H. M.; Sung, M. M. Selective Atomic Layer Deposition of Titanium Oxide on Patterned Self-Assembled Monolayers Formed by Microcontact Printing. *Langmuir* **2004**, *20* (6), 2257–2260.
(20) Lecordier, L.; Herregods, S.; Armini, S. Vapor-Deposited Octadecanethiol Masking Layer on Copper to Enable Area Selective Hf3N4 Atomic Layer Deposition on Dielectrics Studied by in Situ Spectroscopic Ellipsometry. *J. Vac. Sci. Technol. A* **2018**, *36* (3), 031605.
(21) Stevens, E.; Tomczak, Y.; Chan, B. T.; Sanchez, A.; Parsons, G. N.; Delabie, A.; Leuven, K. Area-Selective Atomic Layer Deposition of TiN, TiO2 , and HfO2 on Silicon Nitride with Inhibition on Amorphous Carbon. *Chem. Mater.* **2018**, *3D*, 3223–3232.
(22) Sinha, A.; Hess, D. W.; Henderson, C. L. A Top Surface Imaging Method Using Area Selective ALD on Chemically Amplified Polymer Photoresist Films. *Electrochem. Solid-State Lett.* **2006**, *9* (11), G330–G333.
(23) Sinha, A.; Hess, D. W.; Henderson, C. L. Transport Behavior of Atomic Layer Deposition Precursors through Polymer Masking Layers: Influence on Area Selective Atomic Layer Deposition. *J. Vac. Sci. Technol. B Microelectron. Nanom. Struct.* **2007**, *25* (5), 1721.